JACS
JOURNAL OF THE AMERICAN CHEMICAL SOCIETY
Article
pubs.acs.org/JACS

Mechanisms of Oxidase and Superoxide Dismutation-like Activities of Gold, Silver, Platinum, and Palladium, and Their Alloys: A General Way to the Activation of Molecular Oxygen

Xiaomei Shen,[†,‡] Wenqi Liu,[§] Xuejiao Gao,[‡] Zhanghui Lu,[†] Xiaochun Wu,[*,§] and Xingfa Gao[*,†,‡]

[†]College of Chemistry and Chemical Engineering, Jiangxi Normal University, Nanchang 330022, China

[‡]CAS Key Laboratory for Biomedical Effects of Nanomaterials and Nanosafety, Institute of High Energy Physics, Chinese Academy of Sciences, Beijing 100049, China

[§]CAS Key Laboratory of Standardization and Measurement for Nanotechnology, CAS Center for Excellence in Nanoscience, National Center for Nanoscience and Technology of China, Beijing 100190, China

Supporting Information

ABSTRACT: Metal and alloy nanomaterials have intriguing oxidase- and superoxide dismutation-like (SOD-like) activities. However, origins of these activities remain to be studied. Using density functional theory (DFT) calculations, we investigate mechanisms of oxidase- and SOD-like properties for metals Au, Ag, Pd and Pt and alloys $Au_{4-x}M_x$ (x = 1, 2, 3; M = Ag, Pd, Pt). We find that the simple reaction—dissociation of O_2—supported on metal surfaces can profoundly account for the oxidase-like activities of the metals. The activation (E_{act}) and reaction energies (E_r) calculated by DFT can be used to effectively predict the activity. As verification, the calculated activity orders for series of metal and alloy nanomaterials are in excellent agreement with those obtained by experiments. Briefly, the activity is critically dependent on two factors, metal compositions and exposed facets. On the basis of these results, an energy-based model is proposed to account for the activation of molecular oxygen. As for SOD-like activities, the mechanisms mainly consist of protonation of $O_2^{\bullet-}$ and adsorption and rearrangement of $HO_2^{\bullet}$ on metal surfaces. Our results provide atomistic-level insights into the oxidase- and SOD-like activities of metals and pave a way to the rational design of mimetic enzymes based on metal nanomaterials. Especially, the O_2 dissociative adsorption mechanism will serve as a general way to the activation of molecular oxygen by nanosurfaces and help understand the catalytic role of nanomaterials as pro-oxidants and antioxidants.

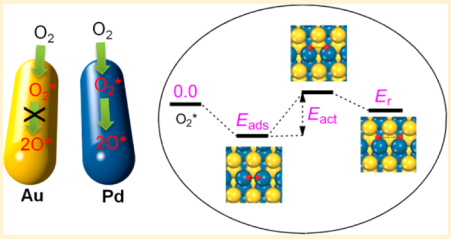

INTRODUCTION

The development and application of nanomaterials as artificial enzyme mimics have attracted much interest. This is because natural enzymes are usually time-consuming to prepare and purify and is subject to easy denaturation and deactivation. In contrast, nanomaterials are much more stable. They are more robust to high temperatures and other harsh reaction conditions and more suited to industrial applications.[1] To date, various nanomaterials have been found to have enzyme-like activities. Especially, they can catalyze some redox-type reactions, acting similarly to natural peroxidase, catalase, oxidase and superoxide dismutation (SOD). According to their chemical compositions, Qu and co-workers have categorized these materials into three kinds: carbon-, metal-oxide-, and metal-based nanomaterials.[2]

Compared with the former two kinds, metal nanoparticles (NPs) possess a larger variety of enzyme-mimetic properties. The same metal NPs can mimic multiple enzymes, depending on the reaction conditions. This provides metal NPs with intriguing environment-responsive ability. As a typical example, Pt NPs can mimic four types of enzymes: peroxidase, catalase, SOD, and oxidase (Figure 1). Pt NPs synthesized using apoferritin as nucleation substrates were able to catalyze the oxidation of 3,3′,5,5′-tetramethylbenzidine (TMB) in the presence of H_2O_2 at pH = 4, acting like peroxidase. In the meantime, they acted like catalase at high pH, catalyzing the decomposition of H_2O_2 to H_2O and O_2.[3] Besides, Kajita et al. reported that pectin-Pt NPs exhibited SOD-like activity to quenching O_2^-,[4] which was employed to reduce oxidative stress

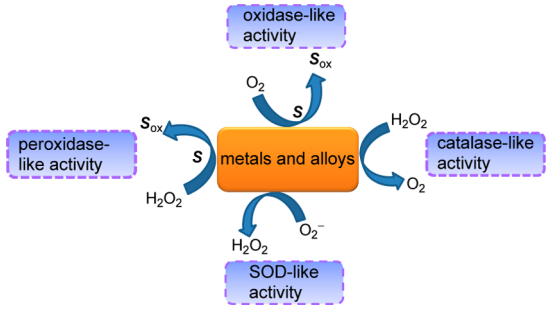

Figure 1. Enzyme mimetic activities of metals and alloys. *S* stands for organic substrates; S_{ox} stands for oxidized organic substrates.

Received: October 3, 2015
Published: December 7, 2015

DOI: 10.1021/jacs.5b10346
J. Am. Chem. Soc. 2015, 137, 15882−15891

caused by reactive oxygen species to extend the lifespan of *C. elegans*.[5] Recently, Yin and co-workers demonstrated the oxidase-like activity for Pt NPs, which catalyzed the oxidation of ascorbic acid in the presence of O_2, similarly to ascorbic acid oxidase.[6] More examples about mimetic enzymes based on metal NPs are summarized in Table 1.[7−18]

Table 1. Enzyme-like Properties Reported for Metal NPs

	Au	Ag	Pd	Pt
peroxidase	ref 7−9	ref 12, 13	ref 14	ref 3, 17, 18
oxidase	ref 10	−	ref 15	ref 3, 6, 17
catalase	ref 11	ref 12	ref 16	ref 4, 17
SOD	ref 11	−	ref 16	ref 4, 16

Another intriguing aspect of metals as enzyme mimics is that they can form alloys with different elemental compositions. This makes it possible to tailor the enzyme-like properties by simply adjusting alloy compositions. Indeed, the oxidase-like activities of PdPt nanodots were found to be composition dependent, which increase with Pt percentage in the alloys.[15] Similarly, the oxidase- and SOD-like activities of Au@PtAg nanorods increase with the Pt percentage.[19]

Despite these progresses, the development of mimetic enzymes with desired properties, which is essential for most practical applications, remains a big challenge.[2] One of the main reasons is that the origins of the enzyme-like activities of metal NPs have been little understood, prohibiting their rational design before synthesis. It is thus necessary to systematically investigate the mechanisms of the enzyme-like activities for metal NPs.

Especially, the oxidase-like activities of metals involve the activation of O_2 by metals, a question actually prevailing in many important reactions, e.g., the room-temperature oxidation of CO and aldehyde by O_2.[20−23] Briefly, O_2 has a triplet ground state. Their reactions with closed-shell molecules involve triplet transition states with high energies. Thus, the direct oxidation of organic compounds with O_2 is usually kinetically hindered, despite the high oxidative capability of O_2. This is known as the spin conservation of O_2.[24] Recently, Xiong and co-workers have demonstrated that the catalytic conversion of O_2 from triplet ($^3O_2$) to singlet ($^1O_2$) by the specific surface facet of Pd is a feasible way to activate O_2.[25] However, because the oxidase-like activities were also observed for metals without the detection of $^1O_2$, a general way for metals to activate O_2 must be waiting to be exposed.

Using density functional theory (DFT) calculations and experiments, we have recently studied the mechanisms of the pH-switchable peroxidase- and catalase-like activities for metals Au, Ag, Pd and Pt.[26] Here, we will study the mechanisms of the oxidase- and SOD-like activities for these metals and their alloys using these approaches. We will report that the dissociative adsorption of O_2 on the metal surfaces to form single-atomic O adatoms is the key step that provides the surfaces with oxidase-like activities. As a proof, the activity orders for metal series predicted by DFT calculations on the basis of this mechanism are in good agreement with the experimental measurements. This dissociative adsorption mechanism serves as a general way to the activation of O_2, for which an energy-based model is further proposed. Interestingly, this model can also be used to explain the previous experimental results about $^1O_2$ harvesting. As for SOD-like activities, the mechanisms mainly consist of protonation of $O_2^{\bullet-}$ and adsorption and rearrangement of $HO_2^{\bullet}$ on metal surfaces. Our results for the first time provide an atomistic-level insight into the oxidase- and SOD-like activities of the metals and alloys and will serve as the basis for the future design and syntheses of novel enzyme mimics based on metal nanomaterials. They will also help understand the pro-oxidant and antioxidant effects of nanomaterials.

CALCULATIONS AND EXPERIMENTS

Calculations. First principle density functional theory (DFT) calculations had been done using Vienna ab initio Simulation Package (VASP).[27−29] The electron−ion interactions were described by using projector augmented wave (PAW) method.[30] The generalized gradient approximation (GGA) was used with the exchange-correlation functional of Perdew-Burke−Ernzerhof (PBE).[31] The performance of PBE in calculating the adsorption energies of O_2 on metal surfaces was tested by comparing the results with those obtained by single-point energy calculations using RPBE[32] and revPBE[33] functionals (see Table S1 of Supporting Information, SI). All geometry optimizations and energy calculations were performed in a plane-wave basis set up to an energy cutoff of 400 eV with a first-order Methfessel−Paxton[34] smearing of 0.2 eV. We employed a four-layered slab in (111) direction with a (3 × 3) unit cell in the lateral direction to model the Au(111) surface. As for the Au(110) and Au(211) surfaces which contain staggered stairs, eight-layered slab along with a (2 × 2) unit cell and six-layered slab with (4 × 2) unit cell were carried for them, respectively. To separate the slab from its periodic images to avoid spurious interaction, a vacuum height of 15 Å along the vertical direction was selected. The calculations were performed using the (3 × 3 × 1), (2 × 2 × 1) and (2 × 4 × 1) Monkhorst−Pack mesh k-points[35] for (3 × 3), (2 × 2) and (4 × 2) unit cells, respectively. Upon geometry optimization, the top one layer of Au(111), the top four layers of Au(110), and the top three layers of Au(211) were fully relaxed, respectively, and the bottom layers were kept fixed. The surface-cleaved method for Pd(111), Pt(111), and Ag(111) surfaces is similar to that for Au(111) surface. Besides, bimetallic alloys composed by Au and other three metals (Pd, Pt, Ag) were investigated. In tailored $Au_{4-x}M_x$ (M = Pd, Pt, Ag) bulk alloys, the contents of other metals were 25%, 50% and 75%, respectively. Consequently, the bulk alloys of Au_3M, Au_2M_2, and AuM_3 (M = Pd, Pt, Ag) were obtained. And $Au_3M(111)$, $Au_2M_2(111)$ and $AuM_3(111)$ surfaces were also cleaved in the similar method of Au(111) surface with (4 × 4) unit cells. Conjugated-gradient algorithm was used to optimize the structures. In all calculations, the convergence criterion of electronic structures was set to 10^{-6} eV, and the atomic positions were allowed to relax until the forces were less than 0.02 eV/Å. The adsorption energies were calculated in the following expressions:

$$E_{ads} = E_{slab+mol} - (E_{slab} + E_{mol})$$

where $E_{slab+mol}$ represents the total energies of the chosen surface with adsorbate on it, and the E_{slab} and E_{mol} denote the bare chosen surface and the adsorbate, respectively. The reliability of the geometry convergence criterion of 0.02 eV/Å was tested by comparing the energies with those obtained by geometry optimizations using a tighter criterion of 0.002 eV/Å (Table S2 of SI). The "climbing images" nudged elastic band (CI-NEB) algorithm[36] was employed to search for transition states (TSs). For the search of TSs, the same force threshold as the geometrical optimization was used. Stretching frequencies were analyzed to characterize the transition states, for which only one imaginary frequency was found for each of them.[37] Bader charge analysis was performed based on electron densities to confirm the effective charge on atoms.[38]

To investigate the dissociative adsorption of O_2 on metal surfaces, both spin polarized and unpolarized PBE functionals were used for the calculations, because O_2 has a triplet ground state. To investigate the adsorption and rearrangement of $HO_2^{\bullet}$ radicals on metal surfaces, only spin unpolarized functional was used. For pure metal surfaces, only spin unpolarized functional was used.

DOI: 10.1021/jacs.5b10346
J. Am. Chem. Soc. 2015, 137, 15882−15891

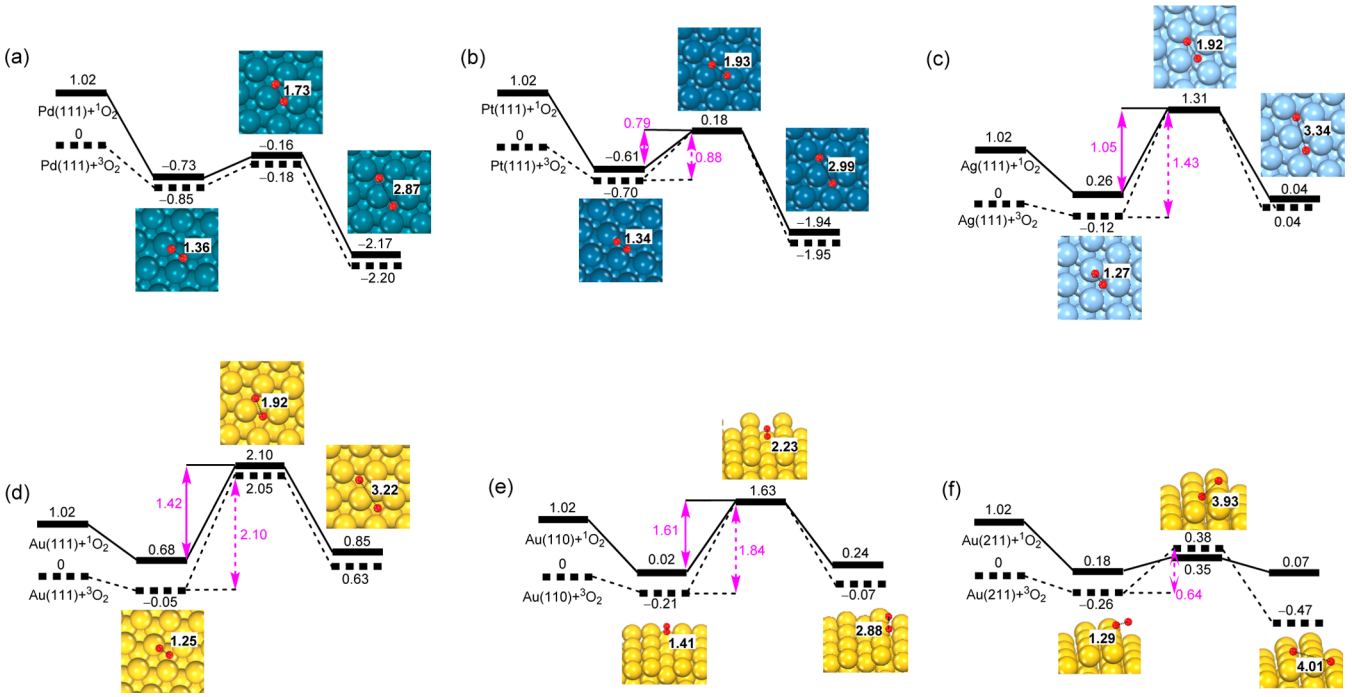

Figure 2. 2D potential energy surfaces for O_2 adsorption and dissociation on facets of (a) Pd(111), (b) Pt(111), (c) Ag(111), (d) Au(111), (e) Au(110), (f) Au(211). The solid and dashed lines are low- and high-spin resulted, respectively. Relative energies (in eV) and O−O atomic distances (in Å) are marked.

Chemicals. Chlorauric acid ($HAuCl_4{\cdot}3H_2O$), potassium(II) tetrachloroplatinate (K_2PtCl_4), palladium chloride ($PdCl_2$), silver nitrate ($AgNO_3$), sodium borohydride ($NaBH_4$), cetyltrimethylammonium bromide (CTAB), L-ascorbic acid (AA), sodium ascorbate (NaA) were all purchased from Alfa Aesar and used as received. Sulfuric acid (H_2SO_4) was purchased from Beijing Chemical Reagent Company. Milli-Q water (18 MΩ·cm) was used for all solution preparation.

Synthesis of Gold Nanorods (NRs). The CTAB-capped gold nanorods were synthesized using a seed-mediated method.[39] After centrifugation twice (9000 rpm, 7 min), the precipitates were redispersed in water and the concentration of GNRs was adjusted to 0.5 mM (gold atom concentration) based on the rod molar extinction coefficient at 400 nm ($A_{400\ nm} = 2020 \times C_{Au}$ (M)) from ref.[40]

Formation of Au@M_1 (M = Au, Ag, AuAg Alloys, Pd and Pt) NRs. In Au@M_x, x means the M/Au ratio. Hereafter, x will be dropped for clarity if $x = 1$. The Au@Au, Ag, AuAg alloys, Pd and Pt NRs were prepared by overgrowth on the GNRs following our previous reports.[41−43] The products were purified by centrifugation (12000 rpm 5 min) twice. Then the precipitates were redispersed in deionized water and the concentration of the NRs was concentrated to 10 nM for further use. The concentration of Au@M NRs is determined by the concentration of GNRs core. Herein, Au@M was employed to investigate oxidase-like activity of different shells. Au@$M_{0.3}$ was used to study the effect of plasmon excitation on NaA oxidation.

Oxidase-like Activities of Au@M Nanostructures Using NaA Oxidation. Ten μL of 10 nM Au@Au, Ag, AuAg alloys were added in 1 mL of deionized water containing 0.1 mM CTAB. Then, 5 μL of 0.01 M NaA was added. In the case of Au@Pd and Pt NRs, 1 μL of 10 nM NRs were added. The reaction kinetics was monitored with 1 min interval by recording the extinction spectra in a scanning kinetics mode.

Effect of Plasmon Excitation on NaA Oxidation. The samples were irradiated with a cw 808 nm laser while keeping reaction temperature at 65 °C for 30 min. The extinction spectra were recorded with 5 min interval. The laser power was 1.145 W measured by a laser power meter.

Characterizations. Extinction spectra were obtained on a Cary 50 UV/vis/NIR absorption spectrometer. Scanning electron microscopy (SEM) images were obtained with a Hitachi S-4800 operating at an acceleration voltage of 15 kV. Elemental analysis was performed with energy-dispersive X-ray spectroscopy (EDX) from SEM. Zeta potentials were obtained using a zeta potential and size analyzer (Malvern, Zeta-sizer nano ZS).

RESULTS AND DISCUSSION

Oxidase-like Activities of Pd, Pt, Ag and Au. Reportedly, single-atomic O adatoms on metal surfaces have Brønsted-base character. They are able to abstract acidic hydrogens from surrounding molecules to act as oxidizing agents. Indeed, it has been demonstrated that gold precovered with O adatoms has strong oxidative capability, being able to oxidize CO and aldehyde.[22,23] Therefore, the following two reactions (eq 1 and eq 2) serve as a plausible mechanism for the oxidase-like activities of metals.

$$O_2 = 2O^* \quad (1)$$

$$O^* + S \rightarrow H_2O^* + S_{ox} \quad (2)$$

Namely, the metals catalyze the dissociation of O_2 to yield O adatoms, which subsequently abstract hydrogens from substrates such as TMB and ascorbic acid, completing the oxidation of the substrates by O_2. In the whole reactions, metals behave like oxidases. Because of the spin conservation,[24] the direct reactions of $^3O_2$ with organic substrates give rise to compounds with nonzero magnetic moments and high energies, and thus are unfavorable in nature. When $^3O_2$ is dissociated into O-adatoms on metals, its bond order is decreased to zero by accepting spin-down electrons from metals, as both antibonding π^* orbitals of $^3O_2$ are already occupied by spin-up electrons. The transfer of spin-down electrons out of the metals leads to an excess number of spin-up electrons on the metals. Therefore, this process essentially

DOI: 10.1021/jacs.5b10346
J. Am. Chem. Soc. 2015, 137, 15882−15891

transfers magnetic moments from $^3O_2$ to the metals, yielding chemically adsorbed O-adatoms with zero magnetic moments. According to the spin conservation rule,[24] these O-adatoms can react with organic substrates to afford stable nonmagnetic compounds. This qualitatively explains the origin of the oxidase-like activities of metals.

To test whether this simple mechanism is able to account for the oxidase-like activities of metals in a quantitative manner, we predicted the activity order for four metals Pd, Pt, Ag and Au and compared the order with that measured by experiments (for the experimental results, see Experimental Verification). For the bulk structure of Pd, Pt, Ag or Au, the (111) facet is more energetically stable than the other facets.[44] Therefore, we first studied the dissociative adsorption of O_2 on the (111) facets for the four metals. We started our investigation by locating the most energetically favorable adsorption configurations of O_2 on the facets. Considering the triplet ground state of O_2, the calculations were performed using a spin polarized DFT method in order to locate the low-energy high-spin states associated with $^3O_2$. The results suggested that these four facets have the similar lowest-energy adsorption configurations for O_2: the adsorbed O_2 lies almost parallel to the surface, with one O located in the hollow face-centered cubic (fcc) site and the other O on top of the metal atom [e.g., see the intermediate structure of Figure 2a for O_2 on Pd(111)].[45−47] The calculated adsorption energies (E_{ads}'s) markedly increase in the order of Pd(111), Pt(111), Ag(111) and Au(111), which are −0.85, −0.70, −0.12 and −0.05 eV, respectively (Figure 2a−d). These adsorption configurations and energies (E_{ads}'s) are consistent with those that have been reported for O_2 on Pt(111) and Ag(111).[46−48] For example, Ford et al. reported that the E_{ads} for O_2 on Ag(111) is −0.12 eV with the PW91 method,[48] which is equal to the E_{ads} we obtained here with the PBE method. These E_{ads}'s suggest that the adsorptions of O_2 become weaker in the order of Pd, Pt, Ag and Au. In the adsorption configurations of Pd, Pt, Ag and Au, the O−O distances decrease as 1.36, 1.34, 1.27, and 1.25 Å (Table S3). However, all the O−O distances are larger than that of free molecular O_2, which is 1.23 Å. This suggests that the adsorption weakens the O−O bond. A stronger adsorption leads to a larger extent of O−O bond elongation. The weakening of O−O bond can be attributed to the filling of the antibonding π^* orbital (i.e., LUMO) of O_2 by electrons transferred from metals during adsorption.[25]

We then calculated the reaction energy profiles for the homolytic cleavages of the adsorbed $^3O_2$ on facets Pd(111), Pt(111), Ag(111) and Au(111) at the ground states, i.e., the high-spin states. The activation energy barriers (E_{act}'s) of the dissociation reactions are 0.67, 0.88, 1.43, and 2.10 eV, respectively; the corresponding reaction energies (E_r's) between the dissociation and adsorption states are −1.35, −1.25, 0.16, and 0.68 eV, respectively (see dashed lines of Figure 2a−d). The low E_{act}'s and largely negative E_r's for $^3O_2$ on Pd and Pt suggest that the dissociations of $^3O_2$ on Pd and Pt (111) facets are both thermodynamically and kinetically favored at ground states and have considerable oxidase-like activity. In sharp contrast, the high E_{act} (1.43 eV) and positive E_r (0.16 eV) for $^3O_2$ on Ag(111) suggests that the dissociation on Ag(111) facet is both thermodynamically and kinetically disfavored. The dissociation of $^3O_2$ on Au(111) has the highest E_{act} (2.10 eV) and E_r(0.68 eV), and so is also kinetically and thermodynamically disfavored. Therefore, $^3O_2$ will be stable on Au and Ag (111) surfaces, hardly showing oxidase-like activity.[49] According to these energetics, the predicted order of oxidase-activity is Pd(111) > Pt(111) ≫ Au(111), Ag(111).

It has been suggested that O_2 molecules can be converted from the high-spin state ($^3O_2$) to the low-spin state ($^1O_2$) by surface plasmon resonance (SPR) of metals,[25,50−54] we further considered the adsorption and dissociation of $^1O_2$ on the four facets. On Pd(111), Pt(111), Ag(111) and Au(111), the E_{act}'s for the $^1O_2$ dissociations are 0.57, 0.79, 1.05, and 1.42 eV, respectively; the E_r are −1.44, −1.33, −0.22 and 0.17 eV, respectively (see solid lines of Figure 2a−d). These E_{act}'s become lower than the corresponding high-spin ones, indicating the dissociation of $^1O_2$ is kinetically easier than that of $^3O_2$. However, the E_{act}'s are still larger than 1 eV for Ag and Au(111) facets. This means the conversion of O_2 from $^3O_2$ to $^1O_2$ will not essentially enhance its dissociation rate on Ag and Au(111). Namely, regardless of SPR excitation that convert $^3O_2$ to $^1O_2$, Pd(111) and Pt(111) will easily catalyze the dissociation of O_2 but Ag(111) and Au(111) will not. In other words, the order of oxidase-activity predicted on the basis of $^1O_2$ dissociation is identical to that predicted on the basis of $^3O_2$ dissociation.

Reportedly, E_{act}'s for the dissociation of small molecules on metal surfaces are approximately proportional to the corresponding E_{ads}'s, following the Brønsted−Evans−Polanyi (BEP) principle. This provides a convenient way to estimate the relative activity of molecules toward decomposition, as the computation of E_{ads}'s is much easier than that of E_{act}'s. We found that the BEP relation also holds for the dissociation of $^3O_2$ and $^1O_2$ on the four facets (Figure 3). This suggests that

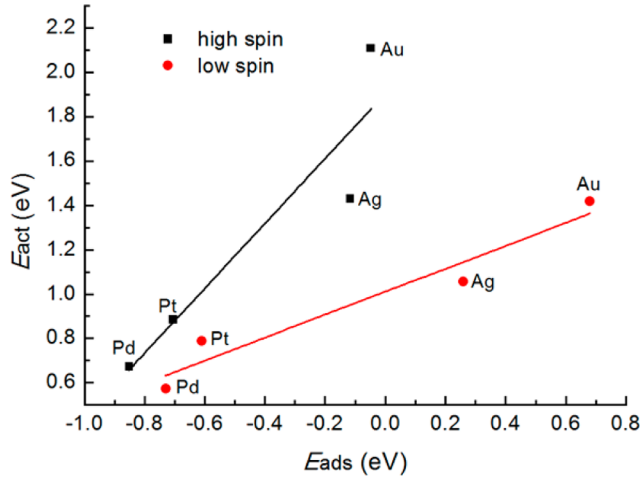

Figure 3. Relation between E_{ads} and E_{act} for O_2 on the (111) facets at low- and high-spin states.

the adsorption strength of O_2 on the facet determines the oxidase-like activity of the facet. A stronger adsorption leads to a large oxidase-like activity. E_{ads} is thus a convenient descriptor for the oxidase-like activity for metals with similar surface structures.

To rationalize the activity order, we calculated the *d*-band centers (ε_d) for the outmost metals in the (111) facet of Pd, Pt, Au and Ag. Positions of those of pure metals are shown with dash lines. According to the *d*-band center (ε_d) theory, the higher the metal's *d* states are in energy relative to the Fermi level, the higher in energy the metal's antibonding states are and thus the higher reactivity of the metal. This theory has been widely used to explain the relative reactivity of metal

DOI: 10.1021/jacs.5b10346
J. Am. Chem. Soc. 2015, 137, 15882−15891

surfaces.[49,55,56] As shown in Figure 4, ε_d of Ag, Au, Pt and Pd are −4.1, −3.5, −2.4 and −1.8. This is in good agreement with the calculated activity order of these four metals Pd(111) > Pt(111) > Au(111), Ag(111). This indicates that the metal's antibonding state plays a primary role in the dissociative adsorption of O_2 and that ε_d is also a feasible descriptor for the oxidase-like activity for the metals.

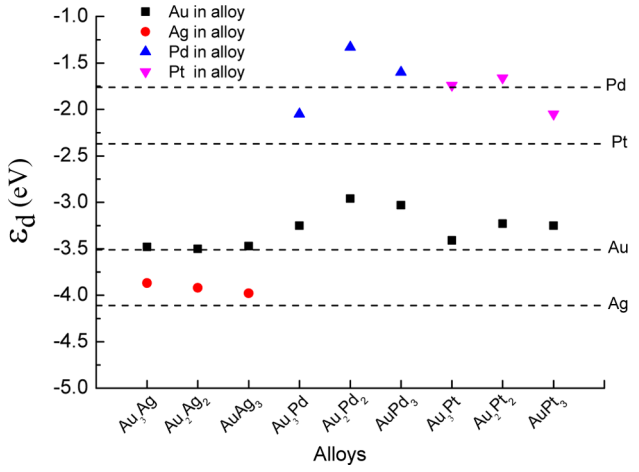

Figure 4. *d*-band centers of metals in (111) facets of alloys.

Facets with higher energies like (100) and (211) may also exist in metal NPs. Therefore, we further studied the oxidase-like activities of Au(110) and Au(211). The E_{act}'s for O_2 on Au(110) are 1.84 and 1.61 eV at high and low spin states, respectively (Figure 2e); the corresponding E_r are 0.14 and 0.22 eV, respectively. This suggests that the dissociative adsorption of O_2 on Au(110) is kinetically and thermodynamically disfavored at either high or low spin state. Au(110) has little oxidase-like activity, as in the case of Au(111). In contrast, the dissociative adsorption of $^3O_2$ on Au(211) is kinetically and thermodynamically favored. The E_{act} is less than 0.4 eV (Figure 2f), indicating a strong oxidase-like activity of Au(211). The (211) facets consist of step structures,[23] which are similar to those abundantly present in NPs of small sizes. This suggests that metal NPs like Au will turn to have oxidase-like activity when their sizes are shrunk to the extent where high-energy facets like (211) become abundant. This is in agreement with

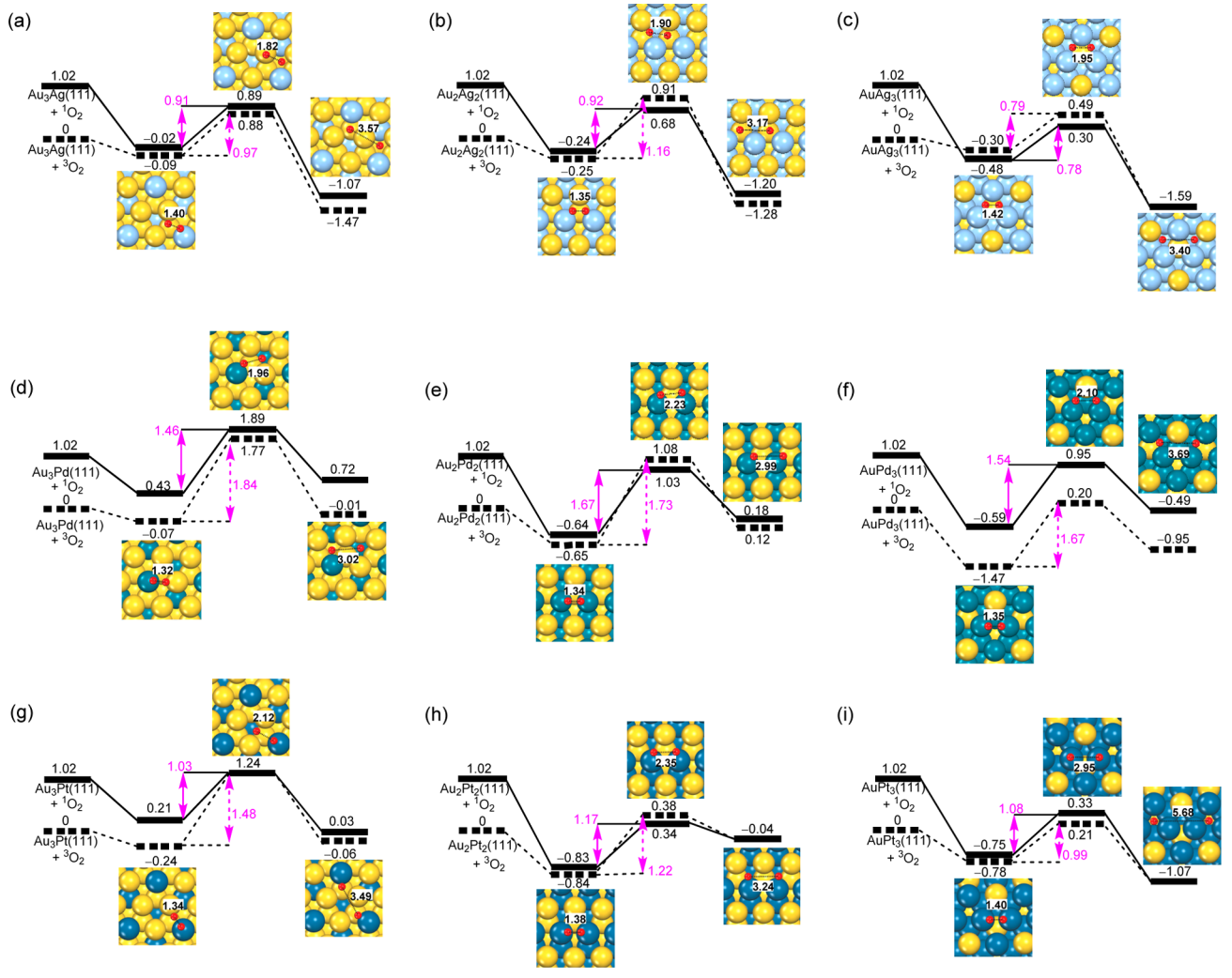

Figure 5. 2D potential energy surfaces for O_2 adsorption and dissociation on (111) facets of (a) Au_3Ag, (b) Au_2Ag_2, (c) $AuAg_3$, (d) Au_3Pd, (e) Au_2Pd_2, (f) $AuPd_3$, (g) Au_3Pt, (h) Au_2Pt_2, (i) $AuPt_3$. The solid and dashed lines are low- and high-spin resulted, respectively. Relative energies (in eV) and O−O atomic distances (in Å) are marked.

DOI: 10.1021/jacs.5b10346
J. Am. Chem. Soc. 2015, 137, 15882−15891

the experimental finding that Au NPs with sizes smaller than 3−5 nm are catalytically active for several chemical reactions, although large Au NPs are chemical inert.[57]

Oxidase-like Activities of Alloys. To verify whether the mechanism of eq 1 and eq 2 is also valid to account for the oxidase-like activity of alloys, we predicted the activity for nine bimetal (111) facets, $Au_{4-x}M_x$ (M = Pd, Pt and Ag; x = 1, 2 and 3). Similarly, we studied the dissociative decomposition of O_2 on these facets at both high and low spin states. Unlike pure metal surfaces, alloy surfaces have more symmetrical unique adsorption sites. Taking $Au_{4-x}Ag_x$ as an example, there exist four, five and four possible adsorption sites for (111) facets of Au_3Ag, Au_2Ag_2 and $AuAg_3$, respectively (Figure S2). All of them were explored here. Table S4 presents the most energetically favorable adsorption sites for O_2 on the (111) facets of Au_3Ag, Au_2Ag_2 and $AuAg_3$.

On the basis of the most energetically favorable adsorption configurations, the corresponding dissociation and transition state configurations were located using DFT calculations at both high and low spin states. The potential energy profiles are present in Figure 5. The E_{ads}'s of O_2 on Au_3Ag, Au_2Ag_2 and $AuAg_3$ at high spin states are −0.09, −0.25 and −0.48 eV, respectively (Figure 5a−c). They are more negative than the corresponding E_{ads}'s for O_2 adsorption on monometallic Au(111) and Ag(111), which are −0.05 and −0.12 eV, respectively. This suggests that (111) facets of AuAg alloys are more reactive than those of monometallic Au and Ag. The corresponding E_{act}'s are 0.97, 1.16 and 0.79, respectively. These barriers are greatly reduced than the E_{act}'s for O_2 dissociation on monometallic Au(111) and Ag(111), which are 2.10 and 1.43 eV. The E_r's are also negative. Therefore, the dissociative adsorption of $^3O_2$ on the (111) facets of Au_3Ag, Au_2Ag_2 and $AuAg_3$ are also thermodynamically favored. The same is true for the dissociation of $^1O_2$ on the facets. This suggests that although Au(111) and Ag(111) facets have little oxidase-like activity, (111) facets of their alloys do have the activity. According to the ground state (high-spin) E_{act}'s, the activity order is $AuAg_3$ > Au_3Ag > Au_2Ag_2.

As for AuPd alloys, the high-spin E_{act}'s for Au_3Pd, Au_2Pd_2 and $AuPd_3$(111) are 1.84, 1.73, and 1.67 eV (Figure 5d−f). That for monometallic Pd is only 0.67 eV (Figure 2a). On the other hand, the E_r's are positive. This means the dissociative adsorption of $^3O_2$ on (111) facets of the alloys are thermodynamically and kinetically disfavored. The same conclusion can been drawn based on the low-spin energetics. Therefore, the mixing of Au into Pd decreases the reactivity Pd. AuPd facets show little oxidase-like activities. This is in sharp contrast to the case of AuAg alloys, in which Au increases the oxidase-like activity of Ag. As for AuPt facets, the activities are also lowered as compared to that of monometallic Pt. The order of oxidase-like activity is Au_3Pt < Au_2Pt_2 < $AuPt_3$ (Figure 5g−i).

Similarly, we calculated the ε_d values for the outmost metals in the facets, intending to study the relationship between the activity and ε_d. As shown in Figure 4, in the AuAg alloys, although the values of ε_d-Au are almost the same with that of monometallic Au, ε_d-Ag values are enhanced. This agrees with the larger activity of AuAg alloys than those of Au and Ag. For AuPd alloys, ε_d-Au and ε_d-Pd in Au_2Pd_2 and $AuPd_3$ both have upshifts with respect to those in pure Au and Pd. However, this disagrees with that the AuPd alloys have decreased activities with respect to that of Pd. Likewise, the shifts of ε_d in AuPt alloys cannot explain the corresponding variation of activities. This suggests that more factors besides metal's antibonding state play roles in the dissociative adsorption of O_2 on alloys, which deserve further study in the future.

SOD-like Activities. Superoxide anion radical $O_2^{\bullet-}$ is a Brønsted base with pK_b = 9.12.[58] Thus, it will easily capture a proton from water to form $HO_2^\bullet$ and OH^-, as illustrated by the following equation

$$O_2^{\bullet-} + H_2O = HO_2^\bullet + OH^- \quad (3)$$

Our calculations suggested that adsorptions of $HO_2^\bullet$ on (111) facets of Au, Ag, Pd and Pt are highly exothermic processes and are facile. The E_{ads}'s are −1.10, −1.52, −1.48, −1.31 eV, respectively. The easy adsorption of $HO_2^\bullet$ will shift the equilibrium of reaction 3 to the right. Therefore, we studied the rearrangements for the adsorbed $HO_2^\bullet$ groups. The results suggested that $HO_2^\bullet$* can easily rearrange to give H_2O_2* and O_2* (eq 4).

$$2HO_2^\bullet* = O_2* + H_2O_2* \quad (4)$$

For example, Figure 6 shows the potential energy profiles for the rearrangements on Au(111) and Pt(111) facets. The E_{act}'s

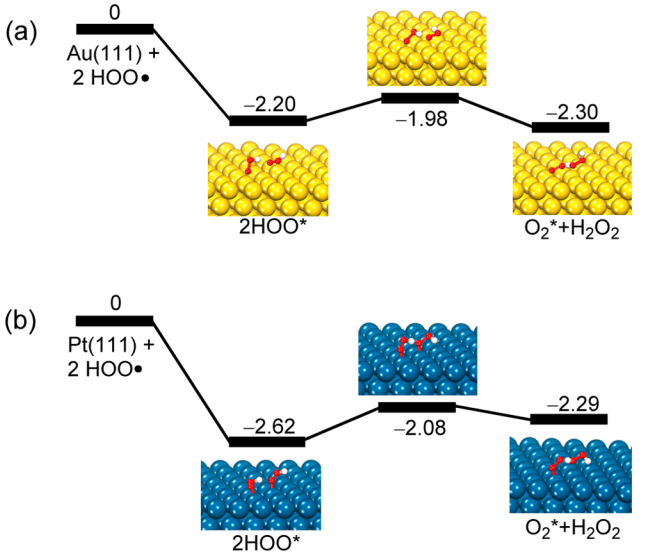

Figure 6. Rearrangements of two $HO_2^\bullet$ groups on (111) facets of (a) Au and (b) Pt.

are very low, which are only 0.22 and 0.54 eV. This means $HO_2^\bullet$* can be readily converted to O_2* and H_2O_2* once they are adsorbed on the surfaces. More discussion about the mechanisms of SOD-like activities is present in part 5 of SI. Thus, eq 3 and eq 4 severe as plausible mechanisms for the SOD-like activities of metals.

Noteworthily, O_2* and H_2O_2* formed in the above processes can undergo further decomposition reactions, depending on the types of the facets and the reaction conditions. Because (111) facets of Au, Ag, Pd and Pt have peroxidase-like activities in acidic conditions and catalase-like activities in basic conditions,[26] H_2O_2* will further decompose to H_2O* and O* in acidic conditions on these four surfaces. In contrast, H_2O_2 will decompose to H_2O and O_2 in basic condition.

Experimental Verification. Herein, we use oxidation of sodium ascorbate (NaA) by dissolved O_2 to characterize the activation of O_2 by metals. Au@M (M = Au, Ag, Pd, Pt) nanorods were used as monometallic samples. At ambient

DOI: 10.1021/jacs.5b10346
J. Am. Chem. Soc. 2015, 137, 15882−15891

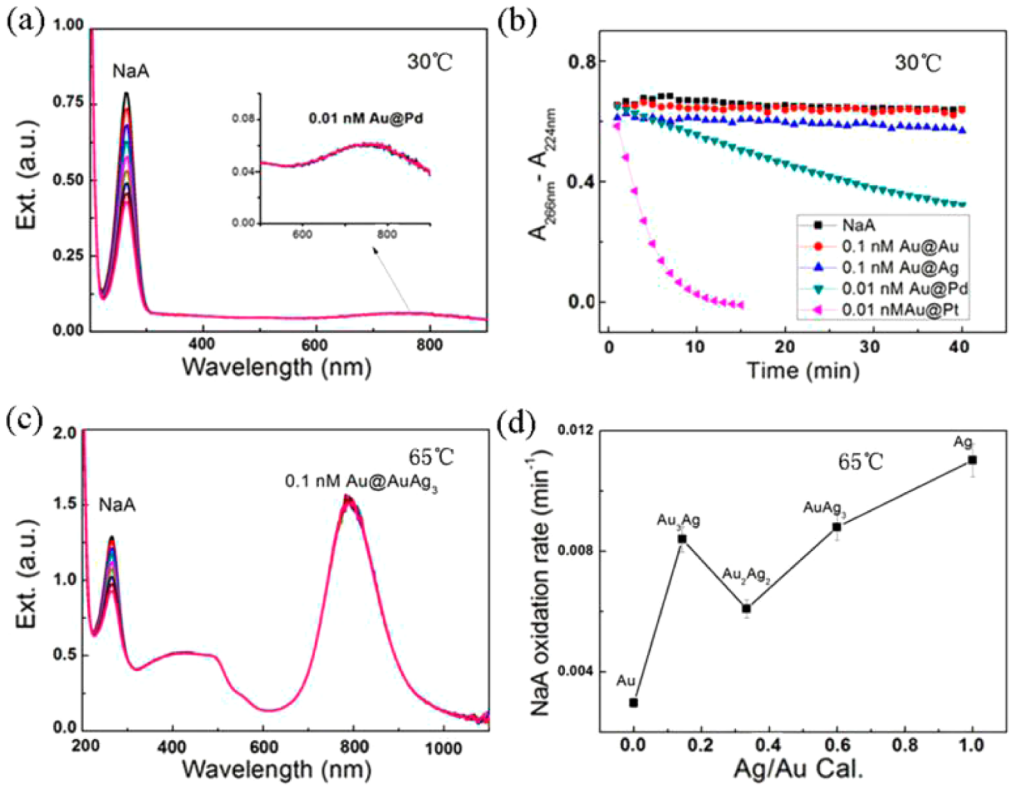

Figure 7. Oxidase-like activities of Au@M (M = Au, Au_3Ag, Au_2Ag_2, $AuAg_3$, Ag, Pd, Pt) nanostructures: extinction spectra evolution during sodium ascorbate (NaA) oxidation catalyzed by Au@Pd NRs at 30 °C (a) or by Au@$AuAg_3$ NRs at 65 °C (c); (b) NaA absorbance change vs reaction time for different shells at 30 °C; (d) NaA oxidation rate at 65 °C vs shell composition. Other reaction parameters: [CTAB] = 0.1 mM, [NaA] = 50 μM.

conditions (30 °C), the catalytic roles of Au@Ag and Au@Au in NaA oxidation can be ignored. In contrast, Au@Pt and Au@Pd show very strong catalytic activity even at 10-fold low rod concentration (Figure 7b and S3). This is consistent with the results predicted using DFT based on the dissociative adsorption mechanism, which suggest that Pd(111) and Pt(111) have considerable oxidase-like activity nevertheless Au(111) and Ag(111) have little. The predicted activity order is Pd(111) > Pt(111) ≫ Au(111), Ag(111). According to Figure 7b, the activity of Pt is stronger than that of Pd, which looks inconsistent with the calculated results. However, Pt prefers the island-growth mode on the Au rods whereas Pd grows epitaxially. Hence, the larger activity of Pt can be ascribed to the larger surface exposure of the Pt shell and probably the introduction of more reactive higher index facets in the islands. Generally speaking, the experimental results efficiently verify the calculated activity order for Au, Ag, Pd, and Pt. The dissociative adsorption of O_2 on metal surfaces is a plausible mechanism to account for the oxidase-like activity of the metals.

In order to probe oxygen activation for alloys, we synthesized Au@M (M = Au_3Ag, Au_2Ag_2, $AuAg_3$) nanorods. Because of the slightly large E_{act} for Au_2Ag_2 (1.16 eV), a high temperature will effectively accelerate the dissociation rate. We thus used the thermal activation by heating reaction solutions involving NaA, dissolved O_2 and the nanorods. As shown in Figure S5, increasing reaction temperature to 45 °C, obvious NaA oxidation appears. Higher reaction temperature is, faster NaA oxidation rate is. Herein, we chose oxidation temperature of 65 °C to study shell composition dependent catalytic behaviors. From Energy Dispersive X-ray Spectroscopy (EDS) analysis, the shell is grown stoichiometrically according to added molar ratios, indicating nearly completely reduction of added ions (Table S6). Au@Au, as predicted by computation, exhibits the lowest activity. After alloying with Ag, the activity is obviously enhanced, consistent with simulation that E_{act} of O_2 dissociation is reduced by alloying. The computed activity order of $AuAg_3$ > Au_3Ag > Au_2Ag_2 agrees well with the experimental one (Figure 7d). Therefore, the dissociative adsorption also efficiently substantializes the oxidase-like activity of AuAg alloys.

An exception in Figure 7d is pure Ag shell. Its experimental catalytic activity is higher than AuAg alloys although the opposite trend is predicted from simulation. The measured Zeta potential of Au@Ag suspension is higher than those of Au@Au and AuAg alloys, indicating more CTAB molecules on Ag shell surface (Figure S7). Increasing CTAB in the suspension decreases NaA oxidation possibly due to occupation of reactive sites by CTAB molecules (Figure S8). We therefore exclude the impact of CTAB adsorption difference. From SEM images, Ag shell exhibits different shape from AgAu alloy shells (Figure S10 of SI). Pure Ag shell has a boat shape due to inhomogeneous overgrowth. It may induce different surface area and exposed facets other than (111) and contributes the high activity of pure Ag.

We also synthesized Au@$M_{0.3}$ (M = Au, Ag, 0.3 is the M/Au molar ratio). Because of the quite thin shells, ligand effects from Au cores were observed.[59] Both Au@$Au_{0.3}$ and Au@$Ag_{0.3}$ show faster NaA oxidation rates than the Au@M_1 samples. For these two Au@$M_{0.3}$ samples, we further studied the effect of light irradiation on NaA oxidation. In agreement with simulation, plasmon excitation indeed enhances the reactivity by slightly reduced O_2 dissociation energy (Figure S9 and Table S7).

The simulation also receives support from previous experimental results. Edwards et al. have reported that acid

DOI: 10.1021/jacs.5b10346
J. Am. Chem. Soc. 2015, 137, 15882−15891

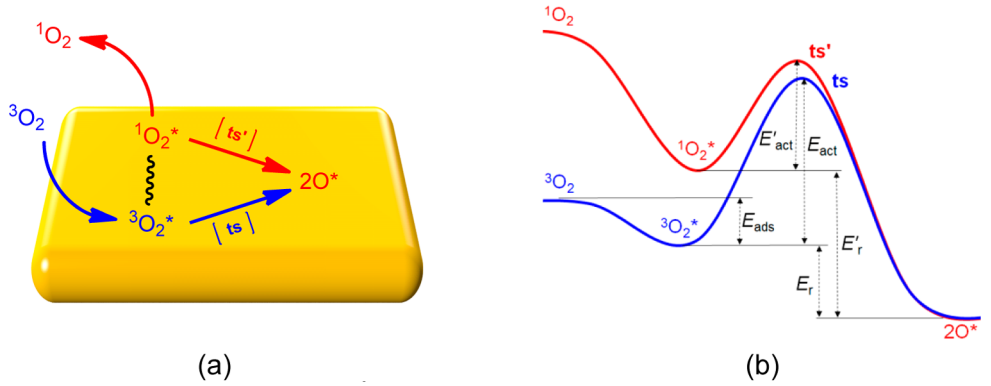

Figure 8. Energy-based model for the activation of $^3O_2$ by metal surfaces: (a) two possible ways to the activation of $^3O_2$ by metal surfaces, formation of O-adatoms and $^1O_2$; (b) typical energy profiles for reactions of (a).

pretreated AuPd alloy supported on carbon switches off the decomposition of H_2O_2 on it, which was supposed that the AuPd alloys were likely to suppress the dissociation of O−O bond of H_2O_2.[60] This experiment is in excellent agreement with our calculated result that alloying Au in Pd makes the dissociation of O−O bond of O_2 both kinetically and thermodynamically disfavored. Hu et al. have reported that Au@PtAg nanorods exhibited oxidase-like activities, which decreases with the increase of Ag percentage in the alloys.[19] Considering that Ag and Au are both group 11 elements, this result is in line with our calculated activity order for AuPt alloys, Au_3Pt < Au_2Pt_2 < $AuPt_3$. Hence, the dissociative adsorption of O_2 on metals surfaces profoundly rationalizes the oxidase-like activities and the activity orders of metals. It provides a general way to the activation of O_2 by metals.

Energy-Based Model for the Activation of $^3O_2$. Besides single-atomic O-adatoms, $^1O_2$ is another important active form of $^3O_2$. Hwang and co-workers have first found that metal NPs (Au, Ag and Pt NPs) can catalyze the photosensitization and generation of $^1O_2$ without the presence of conventional organic photosensitizers.[50] Xiong and co-workers have demonstrated that $^1O_2$ generation is strongly dependent on exposed facets of Pd NPs.[25] Similar morphology dependent formation of $^1O_2$ has been reported for Au and Ag NPs.[51] These findings endow metal NPs with intriguing therapeutic function because of the importance of $^1O_2$ in clinical photodynamic treatments of cancers.

The results we present here can give helpful insights into the facet-dependent generation of $^1O_2$. According to Figure 2 and 5, both $^3O_2$ and $^1O_2$ may dissociate on metal surfaces to afford O-adatoms. Both reaction paths are illustrated in Figure 8a, in which the excitation of $^3O_2$ to $^1O_2$ is also shown. Clearly, $^3O_2$ dissociation and its excitation to $^1O_2$ are two competitive reactions. $^1O_2$, once formed, is also subject to possible dissociation. Shown in Figure 8b are the typical energy profiles for the reactions in Figure 8a, from which several energy-based clues can be derived to predict whether a metal surface is in favor of $^1O_2$ generation. First, a sufficiently negative E_{ads} ensures the stable adsorption of $^3O_2$ on it and is favorable. Second, positive E_r (E_r') is desirable because it means the thermodynamically disfavored dissociation of $^3O_2$ ($^3O_2$). The value of E_{act} (E_{act}') may be less important because the excitation of $^3O_2$ to $^1O_2$ needs large energy, which conquers possible energy barriers.

The above clues can be used to explain the experimentally found facet-dependent generation of $^1O_2$. $^1O_2$ is preferentially formed on Pd(100) over Pd(111) facet.[25] This has been ascribed to that Pd(100) can more efficiently reduce the magnetic moment of adsorbed O_2 by charge transfer than Pd(111), so that O_2 on the former behaves more like $^1O_2$ than that on the latter.[61] According to Figure 2a and Figure S11 of SI, E_r of Pd(111) is much more negative than that of Pd(100) (−1.35 vs −0.97 eV). Namely, $^3O_2$ on Pd(111) will more easily dissociate than that on Pd(100), in line with that Pd(111) is less favorable for $^1O_2$ generation. Therefore, our model provides an alternative explanation in terms of energy. $^1O_2$ is also preferentially formed on Au(110) over Au(111).[51] Similarly, this can be explained using the above model. As shown in Figure 2, the dissociations of $^3O_2$ on both Au(111) and Au(110) are thermodynamically unfavorable because of their positive E_r's (0.68 vs 0.14 eV). The difference is that E_{ads} of $^3O_2$ on Au(111) is much more positive than that on Au(110) (−0.05 vs −0.21 eV). This means $^3O_2$ is only weakly adsorbed on Au(111) and that Au(110) is more favorable for $^1O_2$ generation. Figure 2 shows that Ag(111) has a positive E_r (0.16 eV) and should be favorable for $^1O_2$ generation. Indeed, this has been observed in experiment.[51]

The above experimental results in turn strongly support the validity of the model. Therefore, the model can also be used to predict metal facets that are favorable for $^1O_2$ harvesting. As shown in Figure 5, (111) facets of Au_3Pd, Au_2Pd_2 and $AuPd_3$ all have positive E_r's and will be good candidates for $^1O_2$ formation. So are (111) facets of Au_3Pt and Au_2Pt_2.

CONCLUSION

The oxidase-like activities of nanomaterials consisting of metals (Au, Ag, Pd and Pt) can be effectively rationalized by a simple reaction—dissociation of O_2—supported on the material surfaces. As a proof, the oxidase-like activities, which are assessed by E_{act} and E_r of the reactions available from DFT calculations, are in good agreement with those obtained by experiments. The activity is critically dependent on metal compositions and exposed facets. Au(111) and Ag(111) facets have little oxidase-like activity at low temperatures because O_2 dissociation on both facets are kinetically disfavored at high or low spin state (E_{act} > 1.0 eV). In contrast, Pt(111) and Pd(111) do have the activity because the dissociations on both facets are thermodynamically and kinetically favored (E_{act} < 1.0 eV; E_r < −1.2 eV). For these facets, E_{ads} of O_2 and level of d-band centers are practically more convenient descriptors to estimate the relative oxidase-like activities. High-index facet (211) of even the most inert Au becomes catalytically active.

DOI: 10.1021/jacs.5b10346
J. Am. Chem. Soc. 2015, 137, 15882−15891

Interestingly, alloying Au into the Ag(111) facet markedly "turn on" the oxidase-like activity, despite the inertness of monometallic Au(111) and Ag(111). However, alloying Au into Pd(111) "turns off" the activity of Pd. On the basis of these results, an energy-based model is proposed to account for the activation of molecular oxygen. The model profoundly explains the facet-dependent generation of $^1O_2$ that is experimentally found before and can also be used to design new candidate materials for $^1O_2$ harvesting. On the other hand, mechanisms of SOD-like activities mainly consist of protonation of $O_2^{\bullet-}$ and adsorption and rearrangement of $HO_2^{\bullet}$ on metal surfaces. The results provide an in-depth insight into the oxidase- and SOD-like activities of metals and alloys and provide the basis for optimal tuning the enzyme-like properties of metal nanomaterials by rational design. The dissociative adsorption of O_2 can serve as a general mechanism for the activation of molecular oxygen by nanosurfaces and help understand the catalytic role of nanomaterials as pro-oxidants and antioxidants.

■ ASSOCIATED CONTENT

Supporting Information

The Supporting Information is available free of charge on the ACS Publications website at DOI: 10.1021/jacs.5b10346.

Figures and tables showing the calculated structures, energies, charges, and magnetic moments for species involved in the reactions of this work, figures and tables that characterize metal and alloy nanostructures and their oxidase-like activities. (PDF)

Coordinates for optimized structures. (ZIP)

■ AUTHOR INFORMATION

Corresponding Authors

*wuxc@nanoctr.cn

*gaox@ihep.ac.cn

Notes

The authors declare no competing financial interest.

■ ACKNOWLEDGMENTS

This work was supported by the CAS Hundreds Elite Program, NSFC Project (21373226) and MOST 973 program (2012CB934001).

■ REFERENCES

(1) Wei, H.; Wang, E. K. *Chem. Soc. Rev.* **2013**, *42*, 6060.

(2) Lin, Y. H.; Ren, J. S.; Qu, X. G. *Acc. Chem. Res.* **2014**, *47*, 1097.

(3) Fan, J.; Yin, J. J.; Ning, B.; Wu, X.; Hu, Y.; Ferrari, M.; Anderson, G. J.; Wei, J.; Zhao, Y.; Nie, G. *Biomaterials* **2011**, *32*, 1611.

(4) Kajita, M.; Hikosaka, K.; Iitsuka, M.; Kanayama, A.; Toshima, N.; Miyamoto, Y. *Free Radical Res.* **2007**, *41*, 615.

(5) Kim, J.; Takahashi, M.; Shimizu, T.; Shirasawa, T.; Kajita, M.; Kanayama, A.; Miyamoto, Y. *Mech. Ageing Dev.* **2008**, *129*, 322.

(6) Zhou, Y. T.; He, W. W.; Wamer, W. G.; Hu, X. N.; Wu, X. C.; Lo, Y. M.; Yin, J. J. *Nanoscale* **2013**, *5*, 1583.

(7) Wang, S.; Chen, W.; Liu, A. L.; Hong, L.; Deng, H. H.; Lin, X. H. *ChemPhysChem* **2012**, *13*, 1199.

(8) Jv, Y.; Li, B. X.; Cao, R. *Chem. Commun.* **2010**, *46*, 8017.

(9) Liu, Y. P.; Wang, C. W.; Cai, N.; Long, S. H.; Yu, F. Q. *J. Mater. Sci.* **2014**, *49*, 7143.

(10) Comotti, M.; Della Pina, C.; Matarrese, R.; Rossi, M. *Angew. Chem., Int. Ed.* **2004**, *43*, 5812.

(11) He, W. W.; Zhou, Y. T.; Warner, W. G.; Hu, X. N.; Wu, X. C.; Zheng, Z.; Boudreau, M. D.; Yin, J. J. *Biomaterials* **2013**, *34*, 765.

(12) He, W. W.; Zhou, Y. T.; Wamer, W. G.; Boudreau, M. D.; Yin, J. J. *Biomaterials* **2012**, *33*, 7547.

(13) Jiang, H.; Chen, Z. H.; Cao, H. Y.; Huang, Y. M. *Analyst* **2012**, *137*, 5560.

(14) Lan, J. M.; Xu, W. M.; Wan, Q. P.; Zhang, X.; Lin, J.; Chen, J. H.; Chen, J. Z. *Anal. Chim. Acta* **2014**, *825*, 63.

(15) Zhang, K.; Hu, X. N.; Liu, J. B.; Yin, J. J.; Hou, S. A.; Wen, T.; He, W. W.; Ji, Y. L.; Guo, Y. T.; Wang, Q.; Wu, X. C. *Langmuir* **2011**, *27*, 2796.

(16) Shibuya, S.; Ozawa, Y.; Watanabe, K.; Izuo, N.; Toda, T.; Yokote, K.; Shimizu, T. *PLoS One* **2014**, *9*, e109288.

(17) He, W. W.; Liu, Y.; Yuan, J. S.; Yin, J. J.; Wu, X. C.; Hu, X. N.; Zhang, K.; Liu, J. B.; Chen, C. Y.; Ji, Y. L.; Guo, Y. T. *Biomaterials* **2011**, *32*, 1139.

(18) Liu, J. B.; Hu, X. N.; Hou, S.; Wen, T.; Liu, W. Q.; Zhu, X.; Yin, J. J.; Wu, X. C. *Sens. Actuators, B* **2012**, *166*, 708.

(19) Hu, X. N.; Saran, A.; Hou, S.; Wen, T.; Ji, Y. L.; Liu, W. Q.; Zhang, H.; He, W. W.; Yin, J. J.; Wu, X. C. *RSC Adv.* **2013**, *3*, 6095.

(20) Deng, Q. M.; Zhao, L. N.; Gao, X. F.; Zhang, M.; Luo, Y. H.; Zhao, Y. L. *Small* **2013**, *9*, 3506.

(21) Wahlstrom, E.; Vestergaard, E. K.; Schaub, R.; Ronnau, A.; Vestergaard, M.; Laegsgaard, E.; Stensgaard, I.; Besenbacher, F. *Science* **2004**, *303*, 511.

(22) Gong, J. L.; Mullins, C. B. *J. Am. Chem. Soc.* **2008**, *130*, 16458.

(23) Kim, J.; Samano, E.; Koel, B. E. *J. Phys. Chem. B* **2006**, *110*, 17512.

(24) Behler, J.; Delley, B.; Lorenz, S.; Reuter, K.; Scheffler, M. *Phys. Rev. Lett.* **2005**, DOI: 10.1103/PhysRevLett.94.036104.

(25) Long, R.; Mao, K. K.; Ye, X. D.; Yan, W. S.; Huang, Y. B.; Wang, J. Y.; Fu, Y.; Wang, X. S.; Wu, X. J.; Xie, Y.; Xiong, Y. J. *J. Am. Chem. Soc.* **2013**, *135*, 3200.

(26) Li, J.; Liu, W.; Wu, X.; Gao, X. *Biomaterials* **2015**, *48*, 37.

(27) Kresse, G.; Joubert, D. *Phys. Rev. B: Condens. Matter Mater. Phys.* **1999**, *59*, 1758.

(28) Kresse, G.; Furthmuller, J. *Phys. Rev. B: Condens. Matter Mater. Phys.* **1996**, *54*, 11169.

(29) Kresse, G.; Furthmuller, J. *Comput. Mater. Sci.* **1996**, *6*, 15.

(30) Blöchl, P. E. *Phys. Rev. B: Condens. Matter Mater. Phys.* **1994**, *50*, 17953.

(31) Perdew, J. P.; Burke, K.; Ernzerhof, M. *Phys. Rev. Lett.* **1996**, *77*, 3865.

(32) Hammer, B.; Hansen, L. B.; Nørskov, J. K. *Phys. Rev. B: Condens. Matter Mater. Phys.* **1999**, *59*, 7413.

(33) Zhang, Y. K.; Yang, W. T. *Phys. Rev. Lett.* **1998**, *80*, 890.

(34) Methfessel, M.; Paxton, A. T. *Phys. Rev. B: Condens. Matter Mater. Phys.* **1989**, *40*, 3616.

(35) Monkhorst, H. J.; Pack, J. D. *Phys. Rev. B* **1976**, *13*, 5188.

(36) Henkelman, G.; Uberuaga, B. P.; Jónsson, H. *J. Chem. Phys.* **2000**, *113*, 9901.

(37) Sheppard, D.; Terrell, R.; Henkelman, G. *J. Chem. Phys.* **2008**, *128*, 134106.

(38) Sanville, E.; Kenny, S. D.; Smith, R.; Henkelman, G. *J. Comput. Chem.* **2007**, *28*, 899.

(39) Gou, L. F.; Murphy, C. J. *Chem. Mater.* **2005**, *17*, 3668.

(40) Hu, Z. J.; Hou, S.; Ji, Y. L.; Wen, T.; Liu, W. Q.; Zhang, H.; Shi, X. W.; Yan, J.; Wu, X. C. *AIP Adv.* **2014**, *4*, 117137.

(41) Liu, J. B.; Feng, L. L.; Hu, Z. J.; Hu, X. N.; Hou, S.; Wen, T.; Liu, W. Q.; Zhang, K.; Zhu, X.; Ji, Y. L.; Wang, Q.; Guo, Y. T.; Wu, X. *J. Nanosci. Nanotechnol.* **2013**, *13*, 1006.

(42) Xiang, Y. J.; Wu, X. C.; Liu, D. F.; Jiang, X. Y.; Chu, W. G.; Li, Z. Y.; Ma, Y.; Zhou, W. Y.; Xie, S. S. *Nano Lett.* **2006**, *6*, 2290.

(43) Feng, L. L.; Wu, X. C.; Ren, L. R.; Xiang, Y. J.; He, W. W.; Zhang, K.; Zhou, W. Y.; Xie, S. S. *Chem. - Eur. J.* **2008**, *14*, 9764.

(44) Tyson, W. R.; Miller, W. A. *Surf. Sci.* **1977**, *62*, 267.

(45) Li, W. X.; Stampfl, C.; Scheffler, M. *Phys. Rev. B: Condens. Matter Mater. Phys.* **2002**, DOI: 10.1103/PhysRevB.65.075407.

(46) Eichler, A.; Hafner, J. *Phys. Rev. Lett.* **1997**, *79*, 4481.

(47) Eichler, A.; Mittendorfer, F.; Hafner, J. *Phys. Rev. B: Condens. Matter Mater. Phys.* **2000**, *62*, 4744.

(48) Ford, D. C.; Nilekar, A. U.; Xu, Y.; Mavrikakis, M. *Surf. Sci.* **2010**, *604*, 1565.

DOI: 10.1021/jacs.5b10346
J. Am. Chem. Soc. 2015, 137, 15882−15891

(49) Lima, F. H. B.; Zhang, J.; Shao, M. H.; Sasaki, K.; Vukmirovic, M. B.; Ticianelli, E. A.; Adzic, R. R. *J. Phys. Chem. C* **2007**, *111*, 404.
(50) Vankayala, R.; Sagadevan, A.; Vijayaraghavan, P.; Kuo, C. L.; Hwang, K. C. *Angew. Chem., Int. Ed.* **2011**, *50*, 10640.
(51) Vankayala, R.; Kuo, C. L.; Sagadevan, A.; Chen, P. H.; Chiang, C. S.; Hwang, K. C. *J. Mater. Chem. B* **2013**, *1*, 4379.
(52) Zhao, T. T.; Shen, X. Q.; Li, L.; Guan, Z. P.; Gao, N. Y.; Yuan, P. Y.; Yao, S. Q.; Xu, Q. H.; Xu, G. Q. *Nanoscale* **2012**, *4*, 7712.
(53) Dolmans, D. E. J. G. J.; Fukumura, D.; Jain, R. K. *Nat. Rev. Cancer* **2003**, *3*, 380.
(54) Dougherty, T. J. *Photochem. Photobiol.* **1987**, *45*, 879.
(55) Norskov, J. K.; Bligaard, T.; Rossmeisl, J.; Christensen, C. H. *Nat. Chem.* **2009**, *1*, 37.
(56) Hammer, B.; Nørskov, J. K. *Nature* **1995**, *376*, 238.
(57) Hvolbæk, B.; Janssens, T. V. W.; Clausen, B. S.; Falsig, H.; Christensen, C. H.; Nørskov, J. K. *Nano Today* **2007**, *2*, 14.
(58) Bielski, B. H. J.; Cabelli, D. E.; Arudi, R. L.; Ross, A. B. *J. Phys. Chem. Ref. Data* **1985**, *14*, 1041.
(59) Wang, S. Y.; Kristian, N.; Jiang, S. P.; Wang, X. *Electrochem. Commun.* **2008**, *10*, 961.
(60) Edwards, J. K.; Solsona, B.; N, E. N.; Carley, A. F.; Herzing, A. A.; Kiely, C. J.; Hutchings, G. J. *Science* **2009**, *323*, 1037.
(61) Long, R.; Mao, K. K.; Gong, M.; Zhou, S.; Hu, J. H.; Zhi, M.; You, Y.; Bai, S.; Jiang, J.; Zhang, Q.; Wu, X. J.; Xiong, Y. J. *Angew. Chem., Int. Ed.* **2014**, *53*, 3205.

DOI: 10.1021/jacs.5b10346
J. Am. Chem. Soc. 2015, 137, 15882−15891